

In-situ

K C , W , L ,*, L H , C , L , L ,
W , K E , L L , G , T P J

Gemological Institute, China University of Geosciences, Wuhan 430074, PR China
 Hubei Gem and Jewelry Engineering Technology Research Center, Wuhan 430074, PR China
 School of Materials Science and Engineering, Huazhong University of Science and Technology, Wuhan 430074, PR China
 Mechanical Engineering, University of Birmingham, Birmingham B15 2TT, UK
 School of Electrical and Electronic Engineering, Huazhong University of Science and Technology, Wuhan 430074, PR China
 WMG, Materials Engineering Centre, University of Warwick, CV4 7AL Coventry, UK

ARTICLE INFO

Keywords:

T
C
S
C
B

ABSTRACT

C , - (3DG) . H
(SLM) (3D)
(CVD) C
SLM , 3DG in-situ A CVD
ff) ()
ff . T 3DG/ ff) 88% 27%
(EMI) ff , . P SE 32.3 B EMI ffi-
(SE) 47.8 B 2.7 GH 2-18 GH .
T SLM .

1. Introduction

G , sp^2
(2630 2^{-1}) 1 ,
(2 10^5 2^{-1} V $^{-1}$ -1)
(65000 W $^{-1}$ K $^{-1}$) 2 . H , π - π
(2D)
3 . A
C
(3DG)
fi (60.6 $^{-2}$) 4
(699.7%),
(2DG), 4 , 5 , 6,7 ,
Y (EMI) 8
3DG 9 , 10 ,
11 , 12
H . F
ff 13 . S
()
14 . D
15 . M
CVD
16 . B

*C : G I , C U G , W 430074, PR C .
E-mail address: @ . (.L).

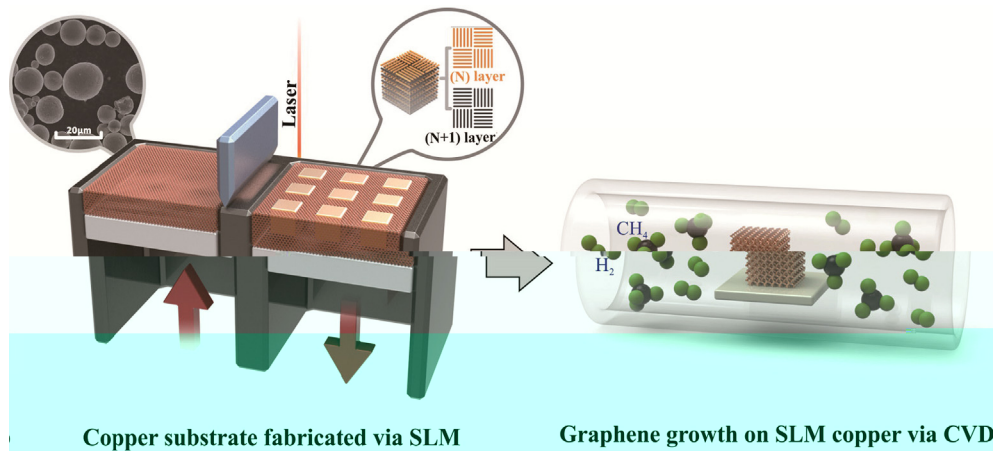


Fig. 1. Schematic diagram of the manufacturing process. The left part shows the SLM process for fabricating a copper substrate. The right part shows the in-situ CVD process for graphene growth on the SLM copper substrate. The diagram includes labels for 'Laser', 'Copper substrate fabricated via SLM', and 'Graphene growth on SLM copper via CVD'. It also features a magnified view of the substrate's surface structure, showing layers labeled '(N) layer' and '(N+1) layer'. The CVD reactor is shown containing CH_4 and H_2 gases.

3. Results and discussion

3.1. Formation of SLM copper

3.1.1. SLM manufacturing of copper under different line energy densities

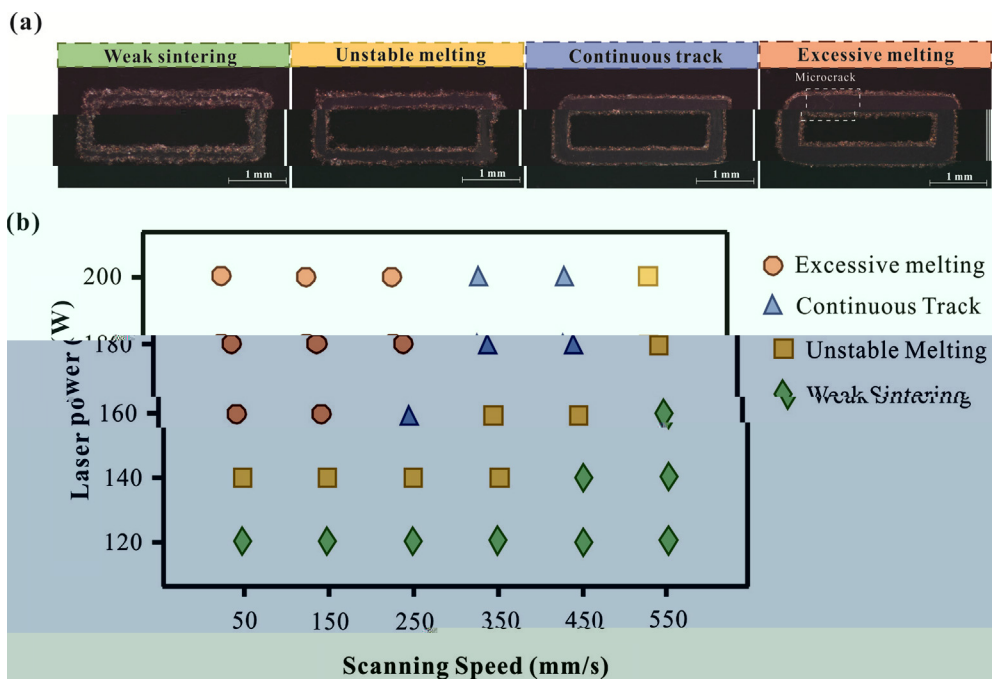


Fig. 2. (a) SEM images of SLM copper tracks under different conditions. (b) Scatter plot showing the relationship between Laser power (W) and Scanning Speed (mm/s) for the four conditions.

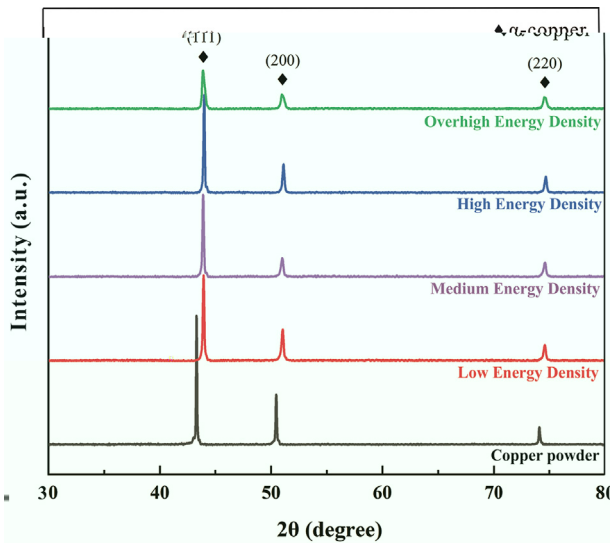


Fig. 3. RD

3.1.2. Formation of anisotropic microstructure under different volumetric energy density

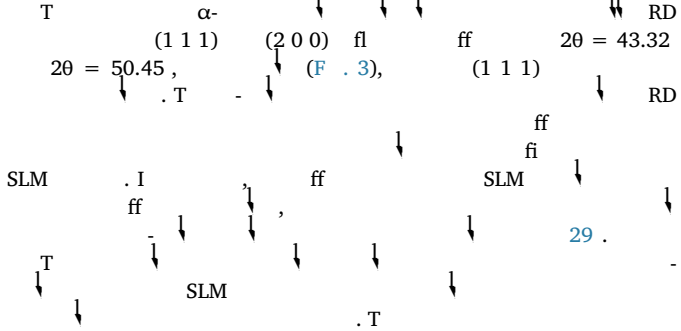
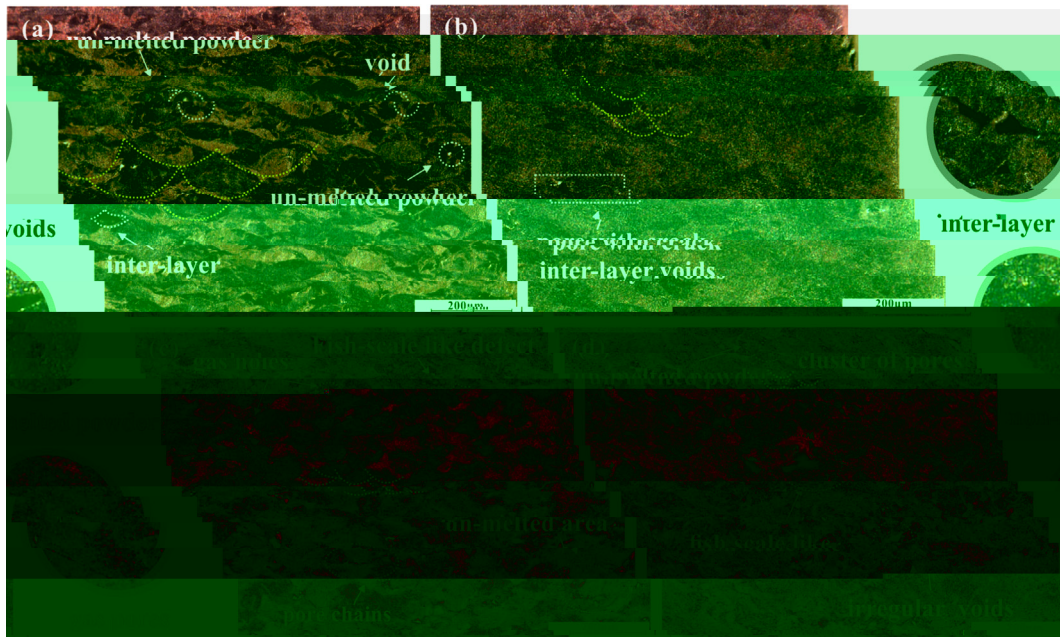


Fig. 4. O (285 J/3), (128 J/3), (3000 J/3), (857 J/3)



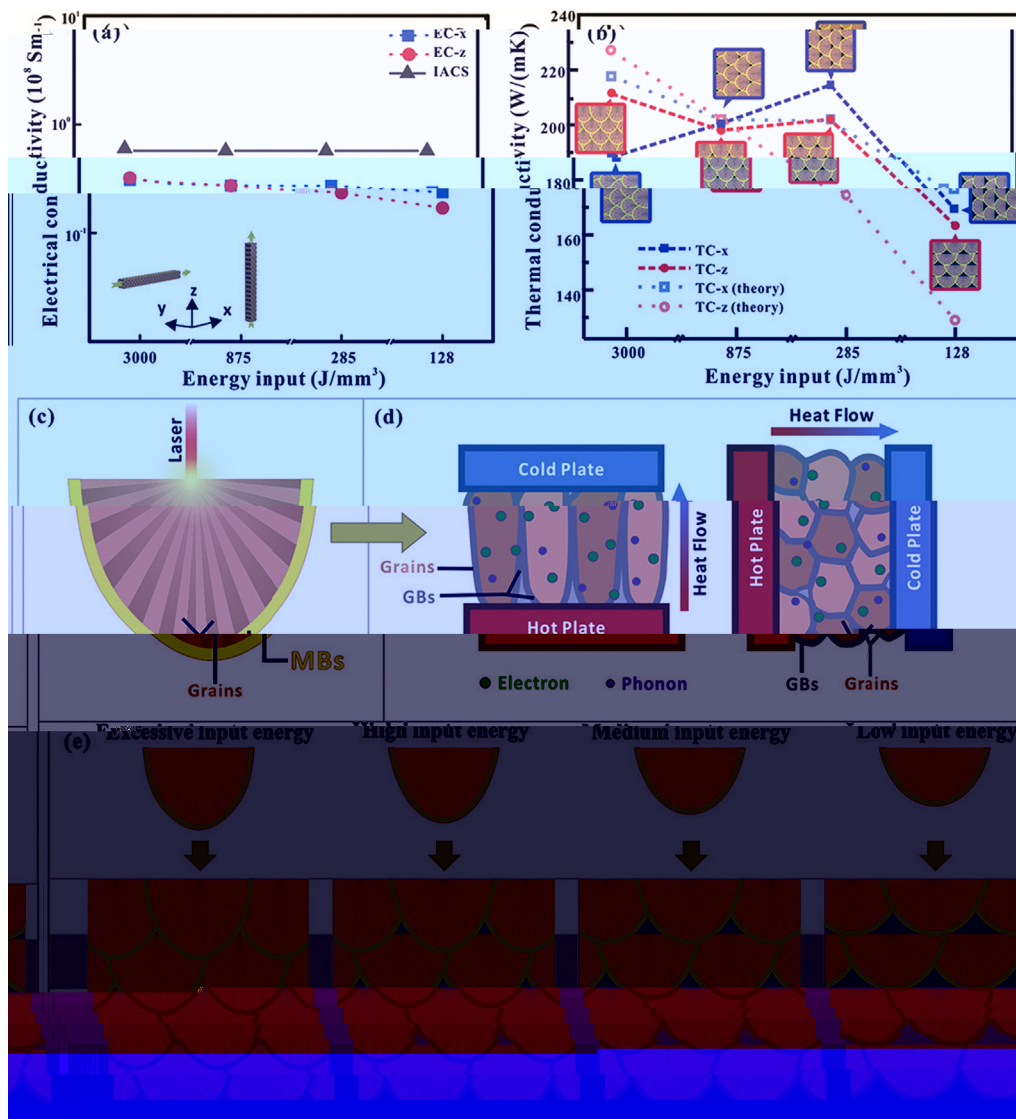


Fig. 7. (a) Electrical conductivity vs. energy input for EC-x, EC-z, and IACS. (b) Thermal conductivity vs. energy input for TC-x, TC-z, and theoretical values. (c) Schematic of laser irradiation. (d) Schematic of heat flow through grains and grain boundaries. (e) Evolution of grain structure under different energy inputs.

3.3. Morphology and structure of CVD 3DG/Cu porous scaffolds

The morphology and structure of CVD 3DG/Cu porous scaffolds were investigated using SEM, EDS, and XRD. The scaffolds were prepared via *in-situ* CVD. The SEM images (Fig. 8a, b) show the porous structure of the scaffolds. The EDS analysis (Fig. 8c-d) confirmed the presence of Cu. The XRD patterns (Fig. 8e-g) show the characteristic peaks of Cu. The pore size distribution (Fig. 8h) shows a narrow distribution around 450 nm. The mechanical properties (Fig. 8i) show a compressive strength of 1590 MPa. The electrical properties (Fig. 8j) show a conductivity of 23 S cm⁻¹. The thermal properties (Fig. 8k) show a thermal conductivity of 42 W m⁻¹ K⁻¹. The microstructure (Fig. 8l) shows a grain size of 43 nm. The porosity (Fig. 8m) is 43%. The surface area (Fig. 8n) is 62699 m² g⁻¹. The pore volume (Fig. 8o) is 0.1350 cm³ g⁻¹. The pore size distribution (Fig. 8p) is centered around 450 nm. The pore size distribution (Fig. 8q) is centered around 450 nm. The pore size distribution (Fig. 8r) is centered around 450 nm. The pore size distribution (Fig. 8s) is centered around 450 nm. The pore size distribution (Fig. 8t) is centered around 450 nm. The pore size distribution (Fig. 8u) is centered around 450 nm. The pore size distribution (Fig. 8v) is centered around 450 nm. The pore size distribution (Fig. 8w) is centered around 450 nm. The pore size distribution (Fig. 8x) is centered around 450 nm. The pore size distribution (Fig. 8y) is centered around 450 nm. The pore size distribution (Fig. 8z) is centered around 450 nm.

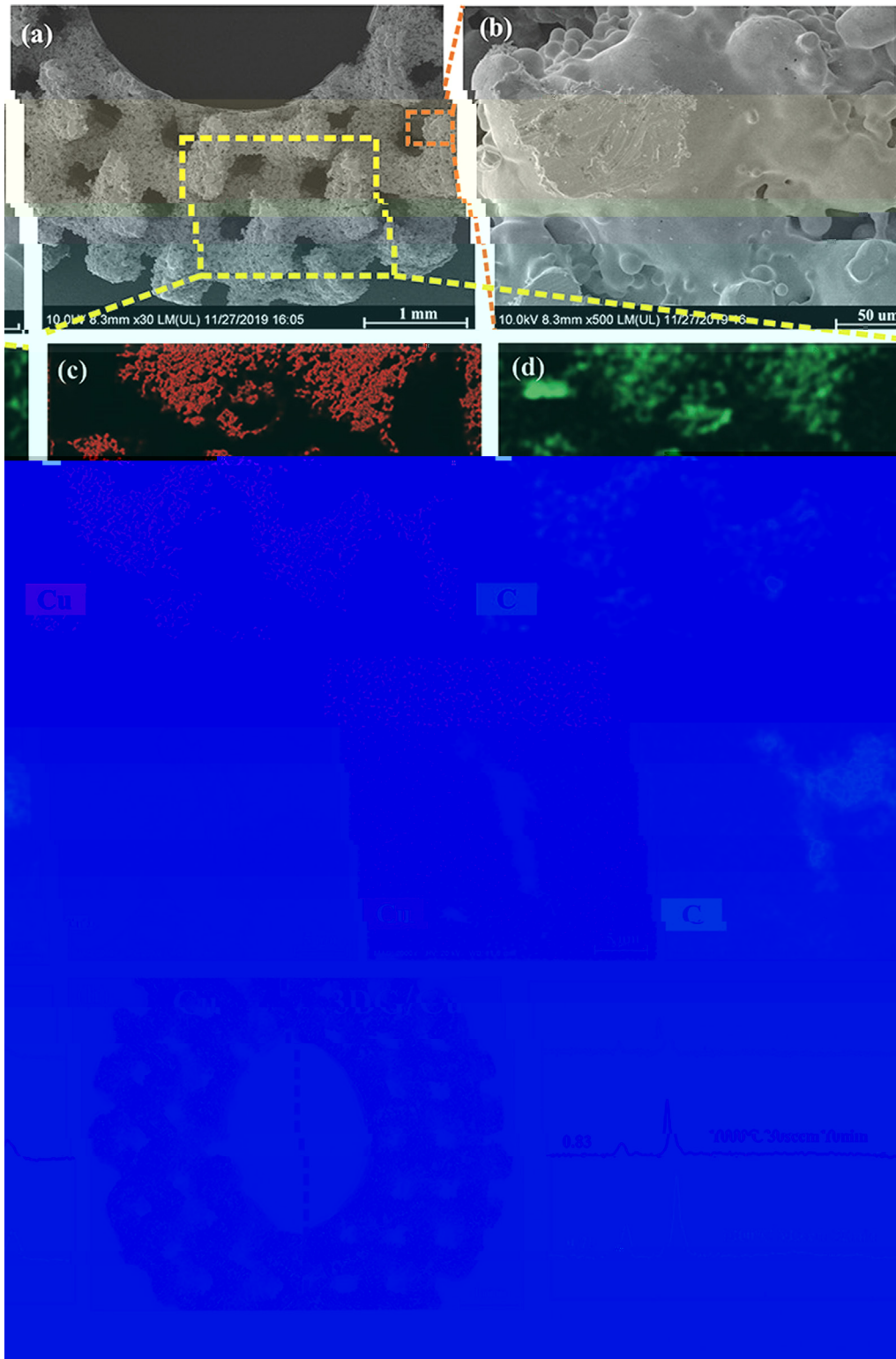


Fig. 8. (a) SEM image of 3DG/Cu porous scaffold at 30x magnification. (b) SEM image of 3DG/Cu porous scaffold at 500x magnification. (c) EDS elemental map for Cu. (d) EDS elemental map for C. The EDS spectrum shows peaks for Cu and C. The intensity ratio I_D/I_G is 0.71. The weight percentage of Cu is 26.8% and the weight percentage of C is 14.8%.

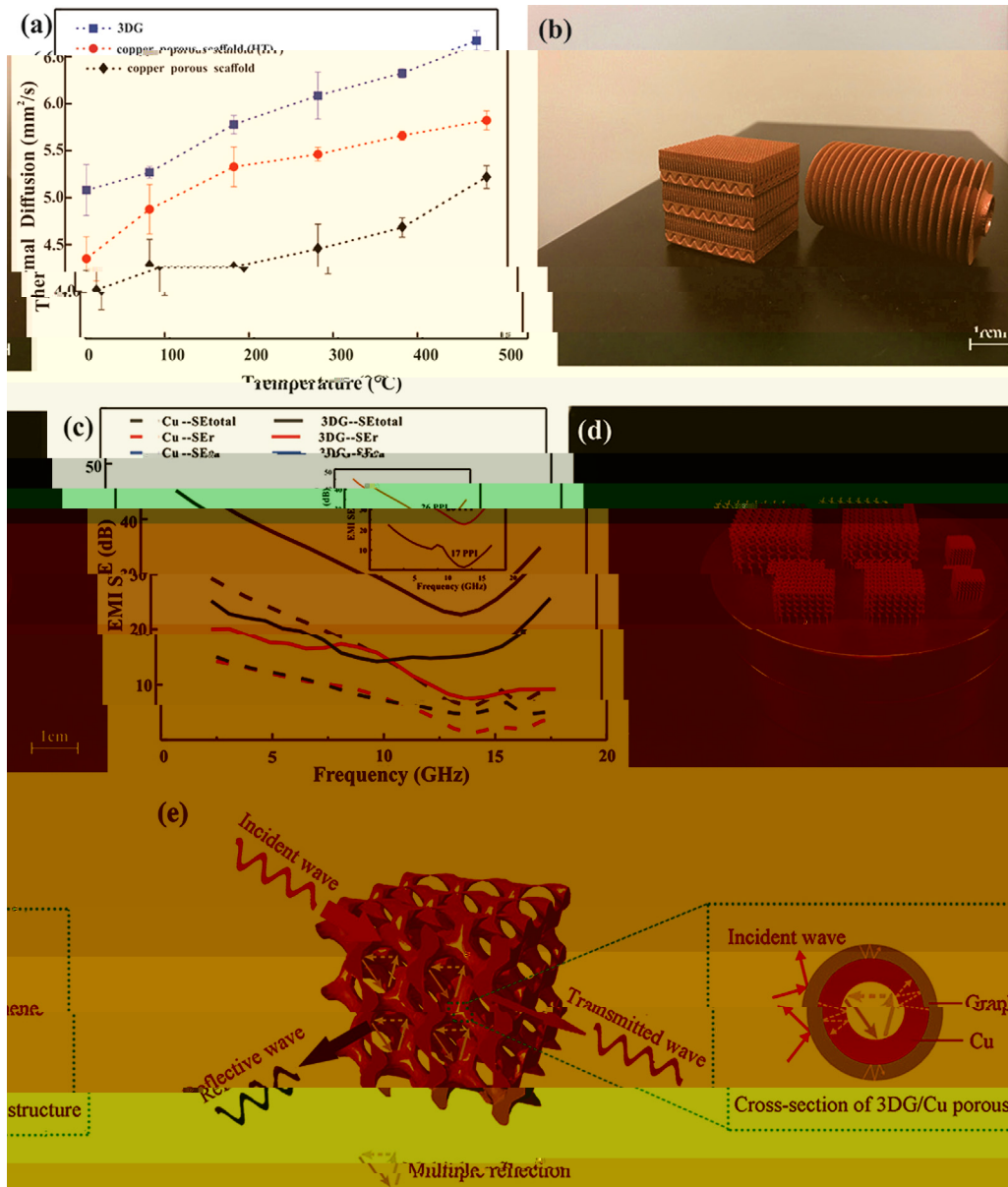


Fig. 9. P 3DG/C ff ; () ff ; () SLM ff ff () S 3DG/C fl EMI. (F

Table 1 C

Coating materials	Substrate	Method	Maximum shielding efficiency (dB)	Improvement of thermal property (%)	Ref
G	G	I + + ↓ + ↓	37	-	50
G	PS	H - ↓ ↓ + ↓ ↓	29.3	-	56
G	PMMA	S ↓ + ↓ +	19	-	57
C /G	/C	S fi + ↓ ↓ ↓	-	8.5	58
G	N	F + CVD	-	554	59
G	C -N	H ↓ + ↓ + ↓	20	-	60
G	C	P + CVD	-	2.4	61
G	C	F - + ↓ ↓	47	6.3	62
G	C	CVD + SLM	47.8	27	T

Note: ↓ (↓ ↓ ↓)-PPMA, ↓ ↓ -PS.

HT
in-situ (F . 9a). S
 3DG/C
 ff
 HT
 1-2
 . I
 fl
 500 μ)
 (F . 9b),
 . G
 (T ↓ 1). I
 N
 T
 EMI, EMI SE,
 (EM)
 2-18 GH (F . 9c),
 ff
 SE
 47.8 B (88.2%)
 3DG/C
 . J K
 133%
 R J V K 45
 . W
 17 26 PPI (F . 9c insert)
 EMI SE. I
 ff
 3DG/C
 32.3 B,
 (30
 3DG/C
 3D
 T
 (SE_a)
 48 . R
 49
 T
 50 . R
 C 51 . F
 52 S O₂ 53 . W

SE_r SE_a
 fi
 F . 9e. W
 3DG/C
 ff
 fl
 3DG/C
 fi
 EM
 fi
 EM
 SE_r. O
 ff
 ff
 J
 54 . I
 fl
 ff . M
 EM
 EM
 . T
 44 . T
 3D
 EM
 CVD
 . I
 R
 S 3.3
 EM
 55 . I
 . O
 3DG/C
 ff
 . T

4. Conclusions

A 3DG/C
in-situ
 ff
 CVD
 ff
 . W
 3DG/C
 EMI SE
 15.9 (
) 32.3 B,
 47.8 B (88.2%)
),
 26.8%
 ff . T
 3DG/C
 fl
 . T
 J
 3DG/C
 EMI
 ff

Credit authorship contribution statement

Kaka Cheng: C
Wei Xiong: V
Yan Li: W &
Liang Hao: F
Zhaoqing Li: V
Yushen Wang: I
Li Lee: D
Ton Peijs: W &
Chunze Yan:
Zhufeng Liu:
Khamis Essa:
Xin Gong: S

53 M 2019;34(5):489-98.
W B, C M, L M. R . A M

54 C H, W S, J , J, C J, S ff F₃O₄
2014;26:3484-9.
2019;121:139-48.
W L, J, Q. T ff MWCNT
-MWCNT . J M S : M B

56 D , P GR, H P, Q F, M B , ML. Effi . J. M
2015;26(3):1895-9.

57 C 2012;22:18772-4.
HB, Q, WG, H , T . ACS A M I

58 S A, U N, T V. T
2011;3:918-24.
M R 2016. :// . /10.1051/ /2016021.

59 P MT, J H, R ff RS, S L. T . N L
2012;12:2959-64.

60 J K, H, H , D . P C -N M L
2017;122:244-7.

61 R H, L S, B S, K TW, L DS, L HJ, T
. S R 2015. :// . /10.1038/ 12710.
T, F SG, L , G Q, L G, R KP, S

62 . M S E A-S 2020. :// . /10.1016/J
.2019.105670.

63 R DA, M LE, M E, H DH, M JL, M BI, . A
N

64 M 2011;59(10):4088-99.
E SF, L KC, S VK, M IC. T . J T
E 1973;1(1):10-38.